Journal of Power Sources 193 (2009) 555–561

Contents lists available at ScienceDirect

Journal of Power Sources

journal homepage: www.elsevier.com/locate/jpowsour

Ethanol oxidation on carbon supported $(PtSn)_{alloy}/SnO_2$ and $(PtSnPd)_{alloy}/SnO_2$ catalysts with a fixed Pt/SnO_2 atomic ratio: Effect of the alloy phase characteristics

E. Antolini[a,b], F. Colmati[b,c], E.R. Gonzalez[b,*]

[a] Scuola di Scienza dei Materiali, Via 25 aprile 22, 16016 Cogoleto, Genova, Italy
[b] Instituto de Química de São Carlos, USP, Av. Trabalhador Saocarlense, 400, C. P. 780, 13560-970 São Carlos, SP, Brazil
[c] Universidade Federal de Goiás – Instituto de Química, C.P. 131, 74001-970 Goiânia, GO, Brazil

ARTICLE INFO

Article history:
Received 23 February 2009
Received in revised form 18 April 2009
Accepted 20 April 2009
Available online 3 May 2009

Keywords:
Ternary alloys
Platinum–tin alloy
Platinum–tin–palladium alloy
Platinum–palladium alloy
Supported catalysts
Ethanol electro-oxidation

ABSTRACT

To evaluate the effect of the alloy phase characteristics on the ethanol oxidation activity, carbon supported $(PtSnPd)_{alloy}/SnO_2$ catalysts were prepared and their electrocatalytic activity compared with that of carbon supported $(PtSn)_{alloy}/SnO_2$. Pt–Sn–Pd/C samples in the atomic ratio (1:1:0.3) and (1:1:1) were characterized by energy dispersive X-ray (EDX) analysis, X-ray diffraction (XRD) and high-resolution transmission electron microscopy (HRTEM). XRD analysis shows the presence of fcc Pt reflexions, shifted to lower angles, and SnO_2 reflexions. By comparison with the XRD patterns of carbon supported Pt–Sn (1:1) and Pt–Pd (3:1) samples, prepared by the same method, the formation of ternary PtSnPd alloys is postulated. The crystallite size of the ternary catalysts is smaller than that of both binary Pt–Sn/C (1:1) and Pt–Pd/C (3:1) catalysts. Chronoamperometry experiments and tests in direct ethanol fuel cells of the as-prepared catalysts shows that the activity for ethanol oxidation of $(PtSn)_{alloy}/SnO_2$ is higher than that of $(PtSnPd)_{alloy}/SnO_2$. This result, obtained with the same Pt/SnO_2 atomic ratio in all the samples, indicates the critical role of the alloy phase characteristics of these catalysts on their activity for ethanol oxidation.

1. Introduction

Low molecular weight alcohols as methanol and ethanol are widely proposed as possible fuels for fuel cells for mobile applications such as electric vehicles [1,2]. The direct oxidation of methanol in fuel cells has been widely investigated. However, the question of the toxicity of methanol remains crucial. Methanol has been known for a long time to be a toxic product, and is associated to possible environmental problems because of its large miscibility with water. On the other hand, ethanol offers an attractive alternative as a fuel in low temperature fuel cells because of its lower toxicity than methanol. Moreover, it can be produced in large quantities from agricultural products and it is the major renewable biofuel from the fermentation of biomass. On these bases the research on direct ethanol fuel cells (DEFCs) is continuously increasing. Carbon supported platinum is commonly used as anode catalyst in low temperature fuel cells. Because catalysis is a surface effect, the catalyst needs to have the highest possible surface area and, for this reason, the active phase is dispersed on a conductive support as carbon. Pure Pt, however, is known to be rapidly poisoned on its surface by strongly adsorbed species coming from the dissociative adsorption of ethanol [3]. Moreover, it has a limited ability for breaking the C–C bond. Preliminary studies indicate that the modification of Pt by tin [1,4] gives very interesting results leading to the oxidation of ethanol at lower potentials than on pure platinum. Conversely to the methanol oxidation, the best binary catalyst for the ethanol oxidation reaction (EOR) in acid environment is not Pt–Ru but Pt–Sn [5]. The optimum Sn content in the catalyst is not well determined, and depends on the ratio of alloyed and non-alloyed tin and on cell temperature [5]. Controversial results regarding the effect of the degree of alloy on the EOR activity of Pt alloy catalysts have been reported. Jang et al. [6] compared the catalytic activity of a partially alloyed Pt–Sn catalyst with that of a quasi non-alloyed $PtSnO_x$ catalyst. From the analysis of results of chronoamperometry and of the performance of direct ethanol fuel cells, the $PtSnO_x$ catalyst showed higher catalytic activity for ethanol electro-oxidation than the Pt–Sn alloy. They deduced that the unchanged lattice parameter of Pt in the $PtSnO_x$ catalyst is favorable to ethanol adsorption and meanwhile, tin oxide in the vicinity of Pt nanoparticles could conveniently provide oxygen species to remove the CO-like species of ethanolic residues to free Pt active sites. In this work, the importance of the presence of a high amount of SnO_2 in the catalyst, with a suitable Pt/SnO_2 atomic ratio, was highlighted. Conversely, Col-

* Corresponding author. Tel.: +55 16 33739899; fax: +55 16 33739952.
E-mail address: ernesto@iqsc.usp.br (E.R. Gonzalez).

0378-7753/$ – see front matter © 2009 Elsevier B.V. All rights reserved.
doi:10.1016/j.jpowsour.2009.04.039

menares et al. [7] observed a high EOR activity for well-alloyed catalysts. They compared the performance of polyol-type Pt/C, Pt–Ru/C (1:1) and Pt–Sn/C (3:1) catalysts with that of the corresponding commercial catalysts. For all catalysts, incomplete ethanol oxidation prevails, and CO_2 formation contributes less than 1% to the products. The EOR activities of the polyol-type catalysts were lower than those of the commercial catalysts, due to a lower activity for acetaldehyde formation. This behaviour was ascribed to a lower degree of alloy in the polyol-type catalysts. Colmati et al. [8] investigated the EOR activity of Pt–Sn/C catalysts (Pt:Sn = 90:10, 75:25 and 66:33) prepared by the formic acid method. They found that the activity of Pt–Sn catalysts for the ethanol oxidation reaction seems to depend on the amount of both non-alloyed and alloyed Sn. The rate determining step for ethanol oxidation depends on the temperature of the reaction and determines the optimal distribution of Sn between the alloyed and non-alloyed states. At low temperatures and/or at low current densities, where the electro-oxidation of ethanol is not fast, the oxidation of adsorbed CO and CH_3CO species determines the rate of the process. In this case the oxidation of ethanol is enhanced by the presence of tin oxides. At high temperatures and high current densities, instead, the rate of ethanol oxidation increases with the increase of the lattice parameter: in the hypothesis of the formation of a Pt–Sn solid solution, a larger lattice parameter should support the cleavage of the C–C bond, or, conversely, the increase of the lattice parameter is associated with an increased number of Pt–Sn pairs, necessary to complete the oxidation of ethanol via acetaldehyde, i.e. without C–C bond cleavage. Tsiakaras [9] correlated the maximum power density (MPD) of DEFCs, using Pt–Sn catalysts with different Pt:Sn atomic ratio as anode materials, with the structural characteristics of the catalysts. A volcano-type curve between the MPD and the lattice parameter of the catalysts, and as a consequence between the MPD and the Sn content in the alloy, was observed, with a maximum at 0.3957 nm for the lattice parameter, and 0.11 for the Sn content. In this work, however, as well as in the works of Colmati et al. [8] and Zhou et al. [10], where comparison of the EOR activity of catalysts with different Pt:Sn atomic ratio was made, simultaneous change in the Pt/SnO_2 atomic ratio and the amount of Sn alloyed occurred. In a separate work, Colmati et al. [11] investigated the activity for ethanol oxidation on as-prepared and thermally treated carbon supported Pt–Sn (1:1) catalysts. Chronoamperometry measurements indicated that the EOR activity of catalysts thermally treated in a reducing atmosphere is lower than that of the as-prepared Pt–Sn/C catalyst. The lower activity of the thermally treated catalysts was ascribed to the absence of SnO_2 in these materials, and clearly demonstrated the importance of the presence of SnO_2 for a high performance of the catalysts. It is also important, however, to evaluate the influence of the alloy phase on the EOR activity, at a fixed Pt/SnO_2 ratio. Indeed, the ratio between the Pt content and the oxide content emerges as another important parameter affecting the EOR activity [12]. In addition to the positive effect of SnO_2 on the activity for ethanol oxidation, as previously reported, the presence of SnO_2 on the particle surface of the Pt–Sn/C catalysts decreases the active surface area of Pt particles. As a consequence, part of the noble metal becomes inactive due to the blocking of the Pt surface by the presence of tin oxide. Comparison of Pt–Sn (1:1) catalysts with different degrees of alloy is not useful because the Pt/SnO_2 atomic ratio is not constant. A method to modify the characteristics of the alloyed phase without changing the Pt/SnO_2 atomic ratio is to insert a third element in the alloy.

Palladium was chosen as a third metal as it fully alloys with Pt [13] and PtPd alloys have the same EOR activity than pure Pt [10,14]. Pd surface segregation commonly takes place in Pt–Pd bulk alloys, but for carbon supported Pt–Pd catalysts with high metal dispersions, as in the present case, Pd segregation is negligible.

2. Experimental

Pt–Sn–Pd/C in the nominal atomic ratios (1:1:0.3) and (1:1:1), Pt–Sn/C (1:1) and Pt–Pd/C (3:1) electrocatalysts were prepared by the so-called formic acid method (FAM). An appropriate mass of the carbon powder substrate (Vulcan XC-72, Cabot, 240 $m^2\,g^{-1}$) is suspended in a 2 mol L^{-1} formic acid solution and the suspension is heated to 80 °C. Chloroplatinic acid ($H_2PtCl_6{\cdot}6H_2O$, Johnson Matthey) solution, a palladium chloride ($PdCl_2{\cdot}2H_2O$, MERCK) solution and a tin chloride ($SnCl_2{\cdot}2H_2O$, MERCK) solution were slowly added to the carbon suspension. The suspension was left to cool at room temperature and the solid filtered and dried in an oven at 80 °C for 1 h. The metal loading was 20 wt.% for all the catalysts.

The atomic ratios of the Pt–Sn/C, Pt–Pd/C and Pt–Sn–Pd/C catalysts were determined by the EDX analytical technique coupled to a scanning electron microscope LEO Mod. 440 with a silicon detector with Be window and applying 20 keV.X-ray diffractograms of the catalysts were obtained at the XRD beam line in the Brazilian Synchrotron Light Laboratory (LNLS), Brazil. The measurements were carried out at room temperature (~25 °C), in the reflection mode, in a 2θ interval from 20° to 120°, in the Cu Kα energy (λ = 0.1539 nm) with a resolution of 4.3 eV, calibrated using Si(1 1 1).

The samples for the HRTEM characterizations were prepared as follows: a carbon film was deposited onto a mica sheet that was placed onto the Cu grids (300 mesh and 3 mm diameter). The material to be examined was dispersed in water by sonication, placed onto the carbon film and left to dry. Histograms of particle sizes were constructed using about 300 particles. This technique was implemented in the Microscopy Laboratory of the Brazilian Synchrotron Light Laboratory using a TEM microscope JEOL, JEM 3010, URP, operating at 300 kV and having a resolution of 0.17 nm.

In order to test the activity for ethanol oxidation, the electrocatalysts were used to make two layer gas diffusion electrodes. A diffusion layer was made with carbon powder (Vulcan XC-72) and 15 wt.% PTFE and applied over a carbon cloth (PWB-3, Stackpole). On top of this layer, the electrocatalyst was applied in the form of a homogeneous dispersion made with Nafion® solution (5 wt.%, Aldrich) and isopropanol (Merck). All electrodes were made to contain 1 mg Pt cm^{-2}.

Chronoamperometry (CA) measurements were performed at 0.8 V for 3600 s. The experiments were done at room temperature with a 1285A Solartron Potentiostat connected to a personal computer and using the software CorrWare for Windows (Scribner).

A stability test was performed by repetitive potential cycling (RPC) between 0 and 1 V. Cyclic voltammograms were recorded in a single cell in 0.5 mol L^{-1} H_2SO_4 solution. Argon (White Martins) was passed for 30 min to eliminate oxygen. Gas diffusion electrodes containing Pt–Sn/C and Pt–Sn–Pd/C electrocatalysts were used as working electrodes. A hydrogen electrode was used as reference and a platinum foil electrode as auxiliary. The CVs were recorded in the range of 0.1–1.0 V vs. a reversible hydrogen electrode (RHE) at a scan rate of 20 mV s^{-1}. The number of cycles was 1000.

For the DEFC studies, the electrodes were hot pressed on both sides of a Nafion® 115 membrane at 125 °C and 50 kg cm^{-2} for 2 min. The Nafion® membranes were pre-treated with a 3 wt.% solution of H_2O_2, washed and then treated with a 0.5 mol L^{-1} H_2SO_4 solution. The geometric area of the electrodes was 4.6 cm^2, and the cathode catalyst was 20 wt.% Pt/C from E-TEK. The cell polarisation data at 60 °C/1 atm and 90 °C/3 atm O_2 pressure were obtained by circulating a 1 mol L^{-1} aqueous ethanol solution at the anode.

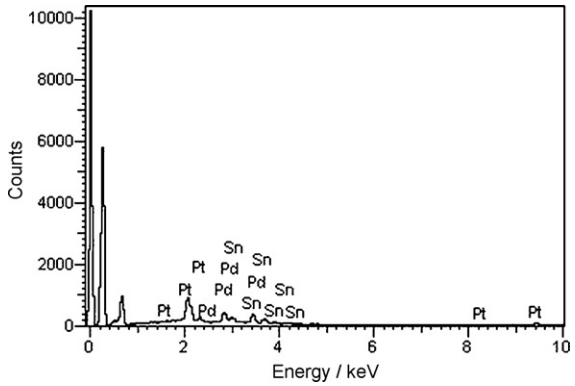

Fig. 1. Typical EDX spectrum of a carbon supported Pt–Sn–Pd (1:1:1) catalyst with 20 wt.% metal loading.

3. Results and discussion

The Pt–Sn–Pd/C catalysts were characterized by EDX measurements on several different regions of each sample of the carbon supported particles. Fig. 1 shows the typical EDX spectrum of the Pt–Sn–Pd (1:1:1) catalyst. The obtained EDX compositions for all the catalysts are shown in Table 1. A slight excess of Sn in both samples, and a slight excess of Pd in the nominal Pt–Sn–Pd (1:1:0.3) with respect to the Pt content was observed.

Fig. 2A shows the XRD patterns of the carbon supported Pt–Sn and Pt–Sn–Pd catalysts prepared by the FAM. The diffraction peak at 20–25° observed in all the diffraction patterns of the carbon supported catalysts is attributed to the (0 0 2) plane of the hexagonal structure of Vulcan XC-72 carbon. As can be seen in Fig. 2A, the XRD patterns of all the catalysts show the characteristic peaks of the face-centered cubic (fcc) crystalline Pt. These diffraction peaks are shifted to lower 2θ values with respect to the corresponding peaks in the pure Pt catalyst. Detailed Pt fcc (3 1 1) peaks of these catalysts are shown in Fig. 2B. The Pt fcc (3 1 1) reflexions of Pt–Pd (3:1) prepared by the FAM and Pt by E-TEK are also reported in Fig. 2B for comparison. The presence of SnO_2 was also detected by XRD analysis. Detailed SnO_2 (2 1 1) peaks of the Sn-containing catalysts are reported in Fig. 2C. No peaks of metallic Pd or Pd oxides were detected in the Pt–Sn–Pd catalysts. The lattice parameters of Pt–Sn–Pd (1:1:0.3) and (1:1:1), Pt–Sn (1:1), Pt–Pd (3:1) and Pt were calculated using the (3 1 1) peak and are reported in Table 1. The value of the lattice parameter of Pt–Sn was larger than that of pure Pt. Radmilovic et al. [16] attributed the value of the lattice constant of 0.3965 nm found for a commercial carbon supported Pt:Sn 1.23:1 catalyst to a mixture of $Pt_{90}Sn_{10}$ (0.3934 nm) and Pt_3Sn phases. Kuznetzov et al. [17], instead, asserted that Pt forms nearly all possible alloys with Sn. Then, the shift of the peaks to lower angles should reveal the formation of a solid solution between Pt and Sn, due to the incorporation of Sn in the fcc structure of Pt. On this basis, assuming that the lattice parameter a follows Vegard's law up to 25 at.% Sn, from the value of the lattice parameter of Pt_3Sn/C by E-TEK (a_s = 0.40015 nm, ca 100% alloyed [18]) and that of Pt/C by E-TEK (a_0 = 0.39206 nm), x (Sn atomic fraction in the PtSn solid solution) was calculated by the relationship:

$$x = \left[\frac{a - a_0}{as - a_0}\right] x_s \quad (1)$$

where x_s is the Sn atomic fraction (0.25) of the Pt_3Sn catalyst. From Eq. (1) it results that the Sn atomic fraction in the PtSn solid solution is 0.16, considerably lower than the stoichiometric value. On the other hand, in the case of the Pt–Pd/C catalyst, a shift of the fcc Pt peaks to higher angles than those of pure Pt was observed. The lattice parameter of the Pt–Pd alloy, calculated from the (3 1 1) peak was 0.3908 nm, between those of pure fcc Pt (a_0 = 0.39206 nm)

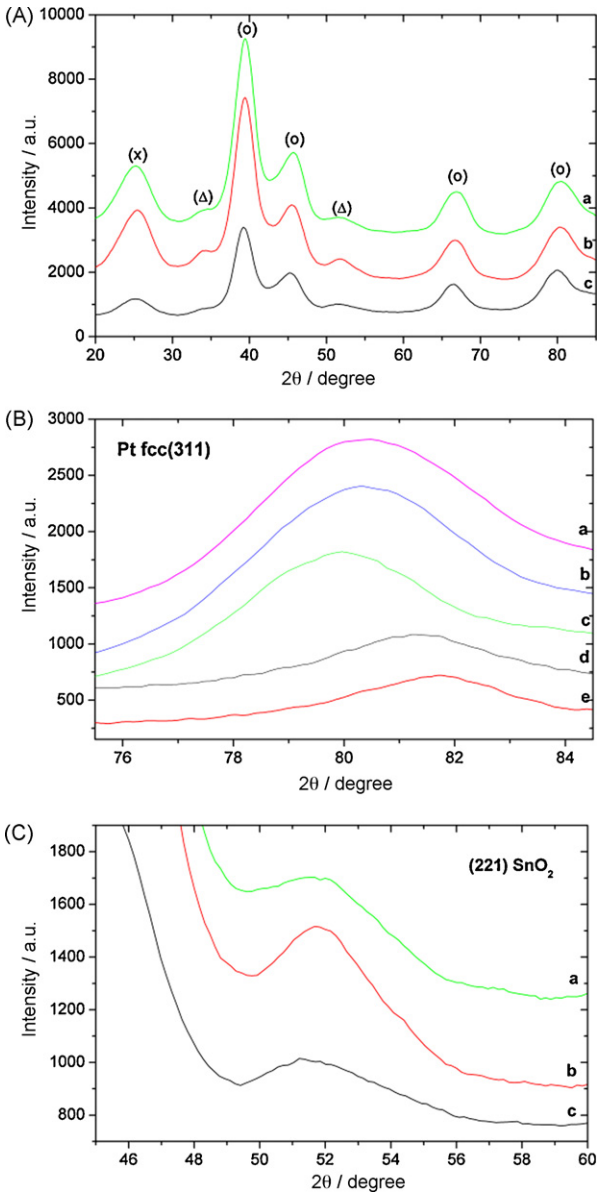

Fig. 2. (A) XRD patterns of carbon supported binary Pt–Sn (1:1) and ternary Pt–Sn–Pd (1:1:0.3 and 1:1:1) catalysts prepared by the FAM. (B) Detailed fcc Pt-alloy (3 1 1) peak. (C) Detailed SnO_2 (2 1 1) peak. (a) Pt–Sn–Pd/C (1:1:1); (b) Pt–Sn–Pd/C (1:1:0.3); (c) Pt–Sn/C (1:1); (d) Pt/C; (e) Pt–Pd (3:1). (○) Pt-alloy; (△) SnO_2, (×) C.

and pure fcc Pd (a_0 = 0.3890 nm). This result indicates that formation of a Pt–Pd alloy occurred. The lattice parameters of the ternary catalysts were larger than that of Pt–Pd/C and smaller than that of Pt–Sn/C. This intermediate value of the lattice parameters of the ternary catalysts can be explained in two ways: (1) a lower amount of Sn alloyed with Pt. Indeed, as observed in other ternary catalysts, the presence of a third non-alloyed metal can cause a decrease of the degree of alloy of the binary base alloy with respect to the binary catalyst [19,20]; (2) the formation of a ternary alloy. Because Pd atoms alloy with Pt atoms, the formation of a ternary Pt–Sn–Pd alloy is likely. To support this hypothesis, as shown in Fig. 3, the lattice parameter of the Pt-alloy linearly decreases with increasing the Pd/[Pt(1 + 0.19) + Pd] atomic fraction in the catalyst, where 0.19 is the Sn/Pt atomic ratio in the alloy from Ref. [15]. Regarding the ternary catalyst Pt–Sn–Pd (1:1:0.3), based on the hypothesis that the amount of Sn and Pd in the ternary alloy are the same than those in the binary catalysts and that the lattice parameter follows Vegard's law, the lattice parameter was calculated by the

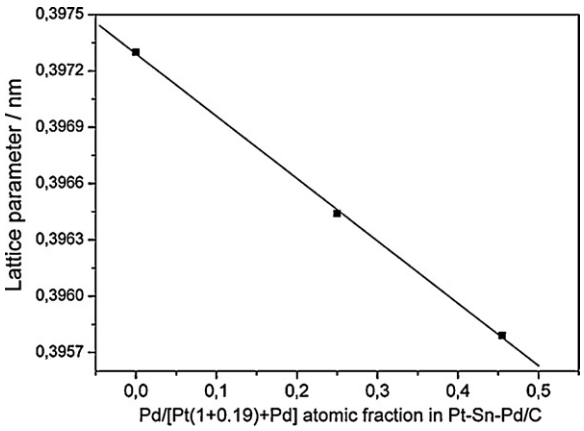

Fig. 3. Pt lattice parameter vs. Pd content in Pt–Sn–Pd/C catalysts.

relationship:

$$a_{PtSnPd} = a_{PtSn} - k_{PtSnPd}x_{Pd} \quad (2)$$

where a_{PtSnPd} is the experimental lattice parameter, a_{PtSn} the lattice parameter of the Pt–Sn/C (1:1) catalyst prepared by the FAM, and x_{Pd} is the atomic fraction of alloyed Pd. In the hypothesis that the dependence of a_{PtSnPd} on the Pd content in the alloy (k_{PtSnPd}) is the same than that of a_{PtPd} on the Pd content in the binary alloy (k_{PtPd}), it follows that:

$$a_{PtSnPd} = a_{PtSn} - k_{PtPd}x_{Pd} = a_{PtSn} + a_{PtPd} - a_{Pt} \quad (3)$$

where a_{PtPd} and a_{Pt} are the lattice parameters of the binary Pt–Pd/C (3:1) catalyst prepared by the FAM, and of Pt by E-TEK, respectively. The value of the lattice parameter calculated from Eq. (3) was 0.39604 nm, in good agreement with the experimental value of 0.39644 nm, attesting the formation of a ternary alloy. In the hypothesis that Pt and Pd form a fcc alloy for all compositions and that it follows Vegard's law, from the relation:

$$a_{Pd} = a_{Pt} - k_{PtPd} \quad (4)$$

using for a_{Pt} the value 0.39206 nm and for a_{Pd} the value 0.3890 nm we obtain a value of the constant k_{PtPd} of 0.00306 nm. In the hypothesis that $k_{PtSnPd} = k_{PtPd}$, and using this value of k_{PtPd}, the atomic fraction of Pd alloyed can be obtained from Eq. (2). The resulting value of x_{Pd} is 0.28. The maximum Pd/[Pt(1 + 0.19) + Pd] atomic fraction in the alloy, where 0.19 is the Sn/Pt atomic ratio in the alloy, is 0.25. The reasonable good agreement between these values means that almost all Pd present in the catalyst is in the alloyed form.

Given the near-coincidence of the Pt and Pt_3Sn reflections and the particle size broadening, an alternative hypothesis is to assume the presence of two Pt-containing phases, Pt_3Sn and Pt, of which only Pt interacts with SnO_2. In this case, the formation of a Pt–Pd solid solution takes place.

The average crystallite sizes of the Pt–Sn–Pd (1:1:0.3) and (1:1:1), Pt–Sn (1:1) and Pt–Pd (3:1) materials were estimated using Scherrer's equation, $d = 0.94k/B\cos\theta$, where d is the average diameter, k the wavelength of X-ray radiation (0.154056 nm), θ the position of the diffraction peak, and B is the width in radians of the diffraction peak at half height. The calculated average crystallite sizes are given in Table 1. As can be seen in Table 1, the crystallite sizes of both ternary Pt–Sn–Pd catalysts are smaller than those of the binary Pt–Sn (1:1) and Pt–Pd (3:1) catalysts prepared by the same method.

Figs. 4 and 5 present the results of the HRTEM analysis of the ternary Pt–Sn–Pd/C catalysts prepared by the FAM. HRTEM micrographs were obtained with magnifications in the range of 150,000–800,000. Low-magnification images (part A of the figures) show that in both catalysts the distribution of the metal particles on the carbon support is uniform and in a narrow particle size range. The histograms of the particle size distribution (part B of the figures), which include analyses of several different regions, reflect quantitatively the uniform distribution in these catalysts. The mean particle diameter, d, was calculated with the following equation:

$$d = \sum(k)\frac{n_k d_k}{n_k} \quad (5)$$

where n_k is the frequency of occurrence of particles with size d_k. The obtained average particle sizes and the corresponding standard deviation for all the catalysts are given in Table 1. The particle size of both ternary Pt–Sn–Pd/C catalysts was considerably smaller than that of Pt–Sn/C (1:1) reported in Ref. [15]. As reported in Ref. [11], the size of the Pt–Sn particles increases for increasing Sn contents in the catalyst. Being constant the total metal load in the catalysts (20 wt.%), the addition of Pd decreases the amount of Sn in the catalyst, resulting in a decrease of the particle size. Part C of Figs. 4 and 5 show high-magnification HRTEM micrographs. The HRTEM images of both catalysts reveal the asymmetric faceted shape, typically cubooctahedral, of the particles. However, in some cases the two-dimensional projection gives the impression of spherical or elliptical shapes.

To compare the potentiostatic behaviour of ternary Pt–Sn–Pd/C and the binary Pt–Sn/C (1:1) catalysts before and after a stability test (repetitive potential cycling (RPC) between 0.1 and 1.0 V), chronoamperometry measurements for ethanol oxidation at 0.5 V were carried out at room temperature and the results are shown in Fig. 6A (as-prepared catalysts) and B (following RPC). It can be clearly seen that the currents for ethanol oxidation on all the catalysts dropped rapidly at first and then became relatively stable. The initial surge of the current is possible due to the charging current. It is clear that the steady state current density for the EOR on the binary Pt–Sn is considerably larger than those on the ternary catalysts. A remarkable effect of the change in the alloy phase by the introduction of Pd atoms in the Pt crystal lattice, at a fixed Pt/SnO_2 atomic ratio, around 1.2, on the EOR activity was observed. At first, the decrease in the EOR activity could be ascribed to the decrease of the lattice parameter, as shown in Fig. 7. However, as reported by Tsiakaras and co-workers [10], in the lattice parameter range 0.3973–0.3958 nm investigated in the present work the maximum power density of a DEFC should increase with a decrease of the lattice parameter of PtSn alloys. The possibility that the higher activity of the catalyst at larger lattice parameters is due to easier cleavage of the C–C bond is remote. As reported in various papers [7,21,22], addition of Sn to Pt catalysts inhibits the C–C bond cleavage. So,

Table 1
EDX compositions, lattice parameters, crystallite size by XRD and particle size by HRTEM of binary Pt–Sn/C (1:1) and Pt–Pd (3:1), and ternary Pt–Sn–Pd/C (1:1:0.3 and 1:1:1) catalysts prepared by the FAM. The lattice parameter and crystallite size of Pt/C by E-TEK are also included.

Catalyst	EDX composition	Lattice parameter from XRD Pt (3 1 1) peak (nm)	Crystallite size by XRD Pt (2 2 0) peak (nm)	Particle size by HRTEM (nm)
PtSnPd (1:1:0.3)	39.4:45.3:15.4	0.39644	2.5	3.1 ± 1.2
PtSnPd (1:1:1)	32.8:34.6:32.6	0.39579	2.4	2.8 ± 0.9
PtSn (1:1)	51:49	0.39730	3.1	6.6 ± 1.7 [15]
PtPd (3:1)	77:23	0.39080	3.4	–
Pt E-TEK		0.39206	2.9	

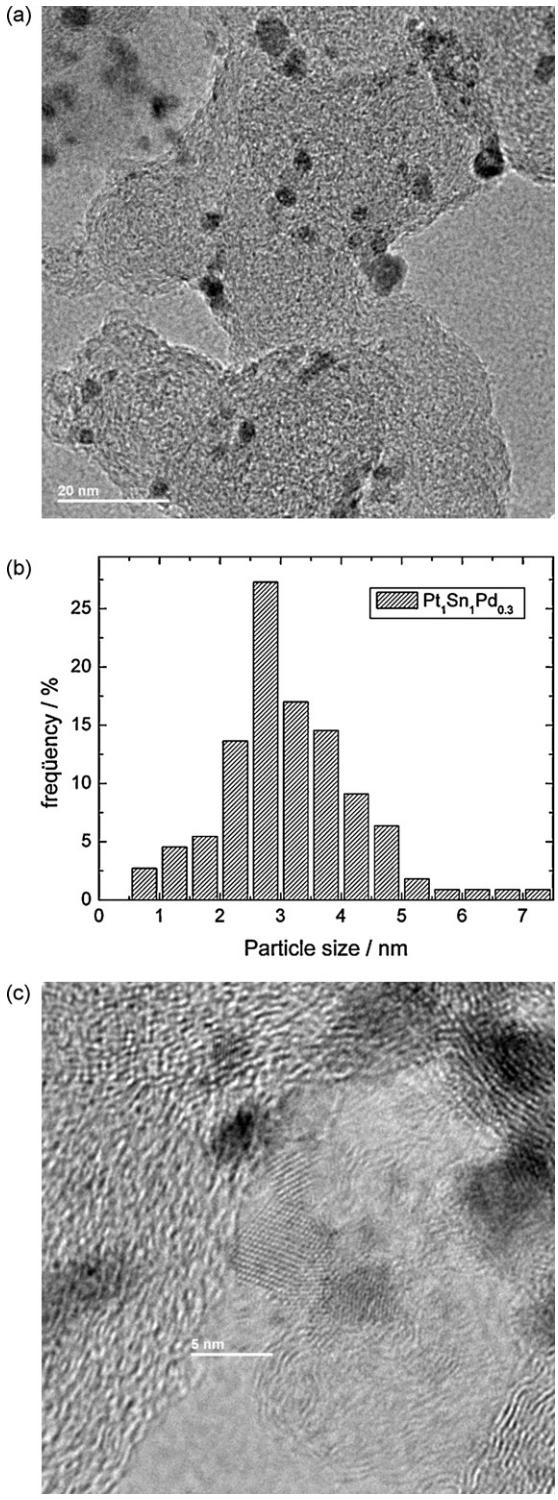

Fig. 4. HRTEM image at low-magnification (A), histogram of particle size distribution (B) and HRTEM image at high-magnification (C) of the catalyst Pt–Sn–Pd/C (1:1:0.3).

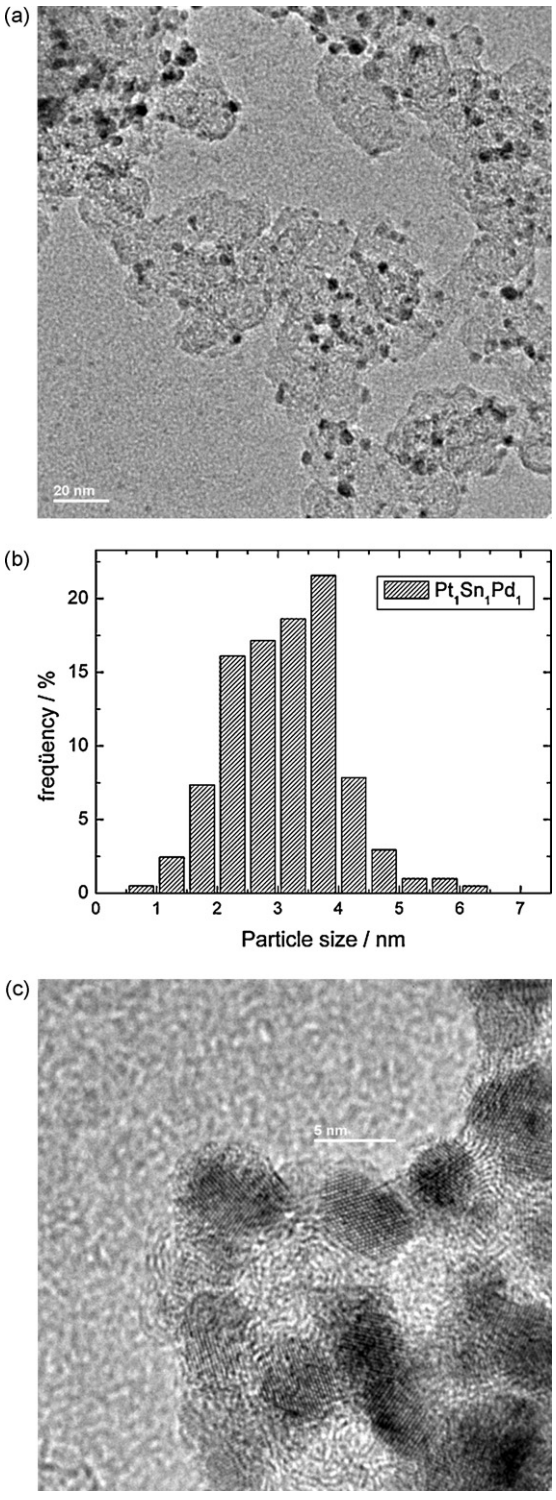

Fig. 5. HRTEM image at low-magnification (A), histogram of particle size distribution (B) and HRTEM image at high-magnification (C) of the catalyst Pt–Sn–Pd/C (1:1:1).

more likely, the decrease of the EOR activity could be related to the increase of the amount of non-active atoms different from Pt in the crystal lattice. This is the case here, because it is known that Pd is inactive for the oxidation of ethanol [23]. As shown in Fig. 8, the EOR activity (steady state current density at 0.8 V from CA) of the as-prepared catalysts decreases for increasing amounts of (Sn + Pd) alloyed. The adsorption of ethanol requires the existence of several adjacent Pt ensembles [4,24] and the presence of heteroatoms around Pt active sites could block ethanol adsorption on Pt sites due to the dilution effect. Therefore, in addition to a suitable Pt/SnO_2 ratio, a low degree of alloy is required to obtain a high EOR activity. Regarding the catalysts submitted to repetitive potential cycling, the difference in the EOR activity of $(PtSn)_{alloy}/SnO_2$ and $(PtSnPd)_{alloy}/SnO_2$ (Pt:Sn:Pd = 1:1:0.3) after RPC was nearly the same (about 82%) than that of as-prepared catalysts. During RPC, loss of oxide and an increase of metal particle size occur, while

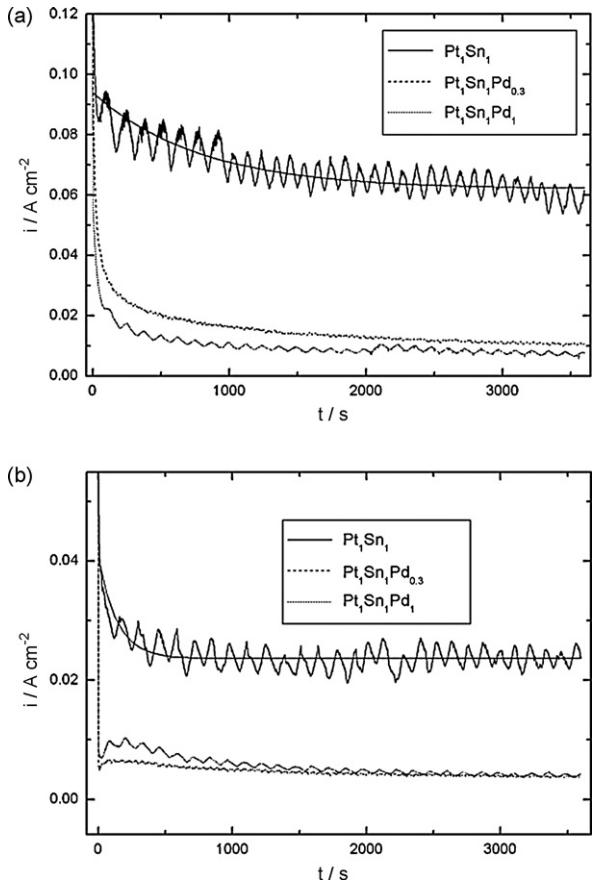

Fig. 6. Chronoamperometry before (A) and after (B) repetitive potential cycling. Continuous line Pt–Sn/C; dashed line Pt–Sn–Pd (1:1:0.3); dotted line Pt–Sn–Pd (1:1:1).

the alloyed phase is generally not affected [25]. So, the difference in the EOR activity after RPC can be ascribed to the difference in the alloy phase, confirming the result obtained with as-prepared catalysts.

The DEFC polarisation curves and power density curves for Pt–Sn/C (1:1) and Pt–Sn–Pd/C (1:1:0.3 and 1:1:1) at 60 and 90 °C are shown in Fig. 9A and B, respectively. At both temperatures, the performance of the cell with the Pt–Sn (1:1) catalyst is better than that of the cells with Pd-containing catalysts, in agreement with the results of CA. The dependence of the maximum power density (MPD) on the amount of alloyed (Sn + Pd) is shown in Fig. 10. At

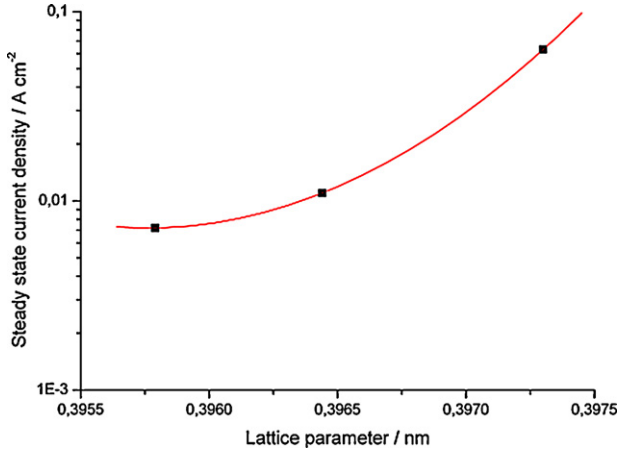

Fig. 7. Dependence of the EOR activity (steady state current density at 0.8 V from CA) of as-prepared catalysts on the lattice parameter.

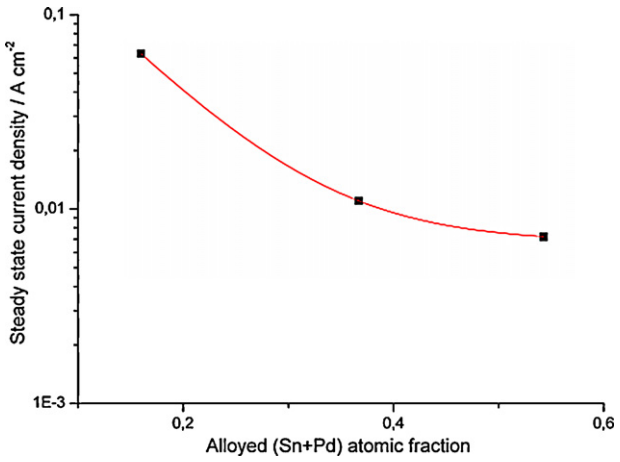

Fig. 8. Steady state current density at 0.8 V vs. alloyed (Sn + Pd) atomic fraction.

60 °C, the MPD almost linearly depends on the (Sn + Pd) content in the alloy and the effect of the Pd presence is less important. On the other hand, at 90 °C the MPD exponentially decays: indeed, the effect of ethanol adsorption on the EOR activity is more relevant at high temperatures. As in the case of methanol oxidation [26], at low temperatures, a lower amount of ethanol is required for the cell operation, because CH_3CH_2OH adsorption is less important. With increasing temperatures the amount of ethanol reacted also

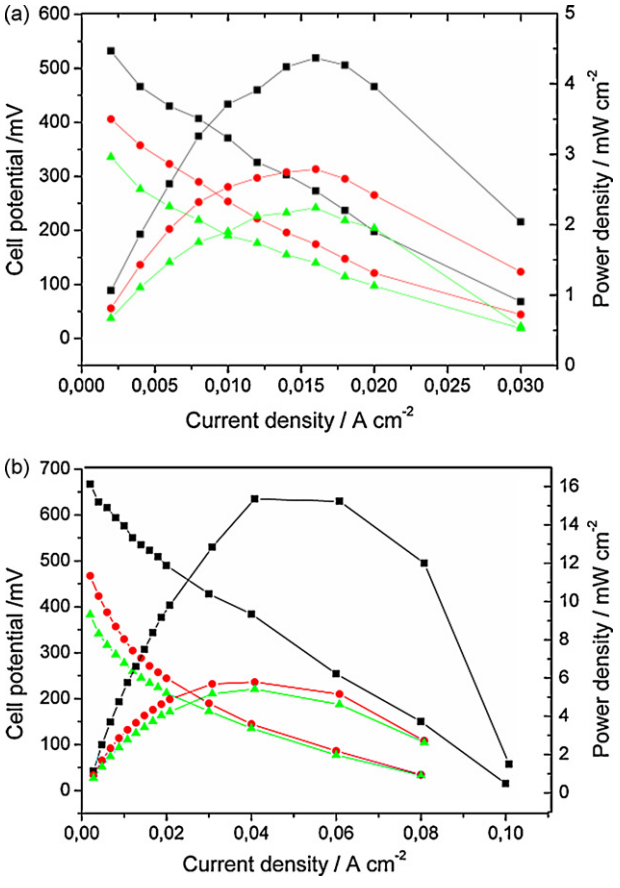

Fig. 9. Current–potential curves and power density curves in single DEFC with binary Pt–Sn/C (1:1) and ternary Pt–Sn–Pd/C (1:1:0.3 and 1:1:1) materials as anode electrocatalysts for ethanol oxidation at 60 °C/1 atm (A) and 90 °C/3 atm (B) O_2 pressure, using a 1 mol L^{-1} ethanol solution. Anode metal loading 1 mg cm^{-2}. Cathode: 20 wt.% Pt/C, Pt loading 1 mg cm^{-2}. (□) Pt–Sn/C (1:1); (○) Pt–Sn–Pd/C (1:1:0.3); (△) Pt–Sn–Pd/C (1:1:1).

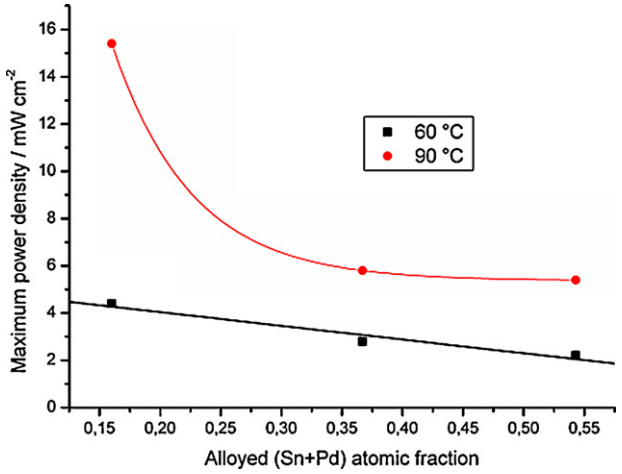

Fig. 10. DEFC maximum power density vs. the alloyed (Sn + Pd) atomic fraction.

increases, and ethanol adsorption becomes the rate determining step of the EOR. Summarizing, the presence of palladium decreases ethanol adsorption and, as a consequence, the activity of the catalysts and the maximum power density of the cell are higher for Pt–Sn than for the Pd containing catalysts.

On the basis of the results obtained in this work, at fixed $(PtSn)_{alloy}/SnO_2$ ratio it is not possible to increase the EOR activity of the catalysts by alloying a third metal, owing to the decrease of ethanol adsorption by the ensemble effect. As a consequence, the only way to increase the EOR activity of $(PtSn)_{alloy}/SnO_2$ is to add a third metal in the oxide form. We prepared a catalyst having better activity than $(PtSn)_{alloy}/SnO_2$ by adding Ru in the oxide form, and the results were reported in Ref. [12]. The activity for ethanol oxidation of $(PtSn)_{alloy}/SnO_2/RuO_x$ was higher than that of $(PtSn)_{alloy}/SnO_2$.

4. Conclusions

Carbon supported ternary Pt–Sn–Pd (1:1:0.3 and 1:1:1) catalysts were synthesized by a formic acid reduction method. From XRD measurements the formation of ternary Pt–Sn–Pd alloys was deduced. The results suggest that Sn atoms partially alloy, while Pd atoms almost fully alloy with Pt atoms. The crystallite sizes of both ternary Pt–Sn–Pd catalysts were smaller than those of binary Pt–Sn (1:1) and Pt–Pd (3:1) catalysts. Chronoamperometry measurements and tests in DEFCs showed a lower activity for ethanol oxidation of ternary Pt–Sn–Pd/C catalysts with respect to binary Pt–Sn/C. This result attests the crucial role of the alloy phase composition on the activity for ethanol oxidation of $(PtSn)_{alloy}/SnO_2$ and $(PtSnPd)_{alloy}/SnO_2$ catalysts, at a fixed Pt/SnO_2 atomic ratio, and indicates that the only way to increase the EOR activity of $(PtSn)_{alloy}/SnO_2$ is to add a third metal in the oxide form.

Acknowledgements

The authors thank the Conselho Nacional de Desenvolvimento Científico e Tecnológico (CNPq, Proc. 310151/2008-2) for financial assistance to the project. Thanks are also due to the Brazilian Synchrotron Light Laboratory for assistance with the XRD and HRTEM experiments.

References

[1] C. Lamy, E.M. Belgsir, J.-M. Léger, J. Appl. Electrochem. 31 (2001) 799.
[2] E. Peled, T. Duvdevani, A. Aharon, A. Melman, Electrochem. Solid State Lett. 4 (2001) A38.
[3] C. Lamy, S. Rousseau, E.M. Belgsir, C. Coutanceau, J.-M. Léger, Electrochim. Acta 49 (2004) 3901.
[4] C. Lamy, A. Lima, V. LeRhun, F. Delime, C. Coutanceau, J.-M. Leger, J. Power Sources 105 (2002) 283.
[5] E. Antolini, J. Power Sources 170 (2007) 1.
[6] L. Jiang, G. Sun, S. Sun, J. Liu, S. Tang, H. Li, B. Zhou, Q. Xin, Electrochim. Acta 50 (2005) 5384.
[7] L. Colmenares, H. Wang, Z. Yusys, L. Jiang, S. Yan, G.Q. Sun, R.J. Behm, Electrochim. Acta 52 (2006) 221.
[8] F. Colmati, E. Antolini, E.R. Gonzalez, J. Electrochem. Soc. 154 (2007) B39.
[9] P.E. Tsiakaras, J. Power Sources 171 (2007) 107.
[10] W. Zhou, Z. Zhou, S. Song, W. Li, G. Sun, P. Tsiakaras, Q. Xin, Appl. Catal. B 46 (2003) 273.
[11] F. Colmati, E. Antolini, E.R. Gonzalez, J. Solid State Electrochem. 5 (2001) 131.
[12] E. Antolini, F. Colmati, E.R. Gonzalez, Electrochem. Commun. 9 (2007) 398.
[13] F.R. de Boer, R. Boom, W.C.M. Mattens, A.R. Miedeama, A.K. Niessen, Cohesion in Metals: Transition Metal Alloys, Elsevier, Amsterdam, 1988.
[14] T. Lopes, E. Antolini, E.R. Gonzalez, Int. J. Hydrogen Energy 33 (2008) 5563.
[15] F. Colmati, E. Antolini, E.R. Gonzalez, J. Alloys Compd. 456 (2008) 264.
[16] V. Radmilovic, T.J. Richardson, S.J. Chen, P.N. Ross, J. Catal. 232 (2005) 199.
[17] V.I. Kuznetsov, A.S. Belyi, E.N. Yurchenko, M.D. Smolikov, M.T. Protasova, E.V. Zatolokina, V.K. Duplayakin, J. Catal. 99 (1986) 159.
[18] F. Colmati, E. Antolini, E.R. Gonzalez, J. Power Sources 157 (2006) 98.
[19] R. Venkataraman, H.R. Kunz, J.M. Fenton, J. Electrochem. Soc. 150 (2003) A278.
[20] Z. Jusys, T.J. Schmidt, L. Dubau, K. Lasch, L. Jorissen, J. Garche, R.J. Behm, J. Power Sources 105 (2002) 297.
[21] S. Rousseau, C. Coutanceau, C. Lamy, J.-M. Leger, J. Power Sources 158 (2006) 18.
[22] R. Alcala, J.W. Shabaker, G.W. Huber, M.A. Sanchez-Castillo, J.A. Dumesic, J. Phys. Chem. B 109 (2005) 2074.
[23] J. Liu, J. Ye, C. Xu, S.P. Jiang, Y. Tong, Electrochem. Commun. 9 (2007) 2334.
[24] H.A. Gasteiger, N.M. Markovic, P.N. Ross, E.J. Cairns, Electrochim. Acta 39 (1994) 1825.
[25] S.C. Zignani, E. Antolini, E.R. Gonzalez, J. Power Sources 182 (2008) 83.
[26] F. Colmati, E. Antolini, E.R. Gonzalez, Electrochim. Acta 50 (2005) 5496.